On Electronic Photoemission from Irradiated C_{60}

P.-G. Reinhard
Institut für Theoretische Physik 2
Universität Erlangen-Nürnberg
Erlangen, Germany

P. Wopperer, P. M. Dinh, E. Suraud
Laboratoire de Physique Théorique
Université Paul Sabatier
Toulouse, France
e-mail: suraud@irsamc.ups-tlse.fr

***Abstract*—We analyze the angular distribution of photoemission (PAD) from irradiated C_{60} clusters focusing on the impact of resonances on emission properties. We make a prospective investigation in terms of a widely used jellium approach, developing an improved version thereof. The jellium allows a simple access in terms of reduced dimension, which is a priori justified by the high degree of symmetry of C_{60}. We show that the PAD is strongly affected by optical resonances, an effect, which would be certainly even enhanced if using a more realistic description of the ionic background.**

Keywords*—C_{60}, *optical resonances, photoemission, jellium model, time-dependent density-functional theory.

I. INTRODUCTION

Photo-induced reactions constitute a key tool to explore the properties of molecules and clusters. Detailed measurements of the emitted electrons provide useful data for analyzing irradiation dynamics. We think here, in particular, of their kinetic energies and angular distributions, coined Photo-electron Angular Distributions (PAD) [1], [2]. Such measurements have a long history in cluster physics [3], [4], [5], [6]. The steady upgrades of light sources and target setups now allow to gather such data with high precision in a large variety of systems [7], [8], [9], and even to analyze dynamical features [9]. Amongst these many studied systems is also the much celebrated fullerene C_{60} [10], which can be viewed as a particularly symmetric large molecule or as a cluster. This interesting system has also been analyzed with respect to photo-emission properties [9]. Although it is rather convenient to handle in experiments, C_{60} remains a demanding object for a theoretical description, particularly if one aims to analyze its dynamics in full detail. However, the increasing number of experimental results calls for more systematic theoretical analysis of the dynamical response to irradiation, especially in terms of the properties of emitted electrons.

In this contribution, we consider, in particular, the PAD on C_{60} and analyze it as a function of laser frequency. The aim is to investigate the relation between PAD and the optical excitation spectrum, especially its resonances. The optical response is the first important observable because it provides the entrance door for the coupling of a system to light pulses. The detailed analysis of the structure of the optical response is thus the crucial first step. In particular, its resonances strongly influence ionization dynamics [11]. For a first exploration, we choose as simple approach a spherical jellium profile as model for the ionic background. This can be justified by the fact that the highly regular shape of C_{60} is close to spherical symmetry and because we restrict ourselves to rather short laser pulses during which ionic motion can be neglected. Moreover, we remind that experiments in gas phase deal with an isotropic ensemble of cluster orientations. This, in turn, requires involved orientation averaging when dealing with detailed ionic background [12]. Spherical jellium represents as such an isotropic system and so provides a simple way to account for the necessary orientation averaging. As a further technical advantage, the spherical jellium background allows us to use a cylindrically symmetric approximation for describing electronic wavefunctions, which represents enormous computational savings and so allows systematic studies. The theoretical description of electrons relies here on Time-Dependent Density-Functional Theory (TDDFT) [13] at the level of Time-Dependent Local-Density Approximation (TDLDA) with the xc-functional of [14] and LDA augmented by an average Self-Interaction Correction [15]. Electronic wavefunctions are discretized on a cylindrical grid and absorbing boundary conditions are used to remove gently the escaping electrons [16], [17], which also provides a simple estimate of the PAD [18].

The paper is outlined as follows: Section II introduces a spherical jellium model for C_{60} with soft jellium boundaries. The obtained values for the Ionization Potential (IP) and the HOMO-LUMO gap are discussed as a function of the model parameters and compared to experimental results. The following section, Section III, discusses the structure of the absorption spectrum determined within the TDLDA approach for the presented jellium model and points out the main features in the spectrum such as resonances and the collective Mie surface plasmon. Section IV analyzes in detail the impact of optical resonances on photoemission observables, e.g., on total ionization and angular distribution of emitted electrons. Thereby, the molecule is irradiated by a femtosecond laser pulse with frequencies tuned around the resonances above the IP.

II. THE JELLIUM BACKGROUND

The spherical jellium model for C_{60} has been used since long because it is an efficient approach for many principle studies, for often used parametrizations see [19], [20]. A slight disadvantage of these jellium models is that they deliver an electronic shell closure at electron number $N_{\rm el} = 260$, rather far away from the experimental $N_{\rm el} = 240$. (The latter comes from the fact that each carbon atom provides 4 valence electrons taking part in binding which altogether make 240 active electrons.) Not only this, the steep jellium boundaries are not well suited for computations using a grid representation as we do.

In order to have a robust jellium model usable on finite size meshs, the model should display a smooth transition from the homogeneous bulk density to zero. This can be achieved

 ISBN: 978-1-61208-303-2

TABLE I. POTENTIAL PARAMETER v_0, IP AND HOMO-LUMO GAP FOR THE THREE DIFFERENT SURFACE WIDTHS σ UNDER CONSIDERATION. THE LAST LINE INDICATES THE EXPERIMENTAL VALUES FOR IP AND GAP.

σ [a_0]	v_0 [Ry]	IP [Ry]	gap [Ry]
0.5	1.5	0.56	0.16
0.6	1.9	0.56	0.12
0.7	2.38	0.56	0.07
exp.		0.57	0.13

by smoothing the step functions in the steep jellium model to Woods-Saxon profiles leading to the following ansatz for the pseudo-density $\rho_{\rm jel}$ and the pseudo-potential $V_{\rm shift}$ of the jellium model:

$$\rho_{\rm jel}(r) = \frac{3}{4\pi r_s^3}\frac{1}{1+\exp((r-R_0)/\sigma)}\frac{1}{1+\exp((R_i-r)/\sigma)} \quad , \tag{1}$$

$$V_{\rm shift}(r) = v_0\frac{1}{1+\exp((r-R_0)/\sigma)}\frac{1}{1+\exp((R_i-r)/\sigma)} \quad , \tag{2}$$

$$R_0 = R+\frac{\Delta R}{2} \quad , \quad R_i = R-\frac{\Delta R}{2} \quad . \tag{3}$$

The pseudo-density $\rho_{\rm jel}$ is the positively charged counterpart of the electron density forming both together a neutral system. In addition to the Coulomb potential of $\rho_{\rm jel}$, we also consider a pseudo-potential $V_{\rm shift}$, which consists in a localized potential shift to put energetic relations right. Similar as for the previous steep jellium models, we choose $R = 6.7\,a_0$ and $r_s = 1.15236\,a_0$. New is the parameter for the surface width σ. It allows some further fine tuning. But it should also be chosen sufficiently large for numerical convenience. We will consider a series of σ. The jellium width ΔR is to be chosen such that the total charge fits N, i.e.

$$4\pi\int dr\, r^2\,\rho_{\rm jel}(r) = N \quad . \tag{4}$$

Actually, we find with the soft jellium model a shell closure at $N_{\rm el} = 238$, thus very close to the expected value of $N_{\rm el} = 240$. Thus we choose for the background $N = N_{\rm el} = 238$. Altogether we have the model parameters

$$N = 238\ ,\ r_s = 1.15236\,a_0\ ,\ R = 6.7\,a_0 \quad \sigma = 0.5,\ 0.6,\ 0.7\,a_0 \quad . \tag{5}$$

The radius width ΔR is adjusted according to condition (4). We consider three models with surface widths $\sigma = 0.5$, 0.6, and $0.7\,a_0$. The strength v_0 of the potential shift depends on σ. The v_0 is listed in Table I together with IP and HOMO-LUMO gap. The table shows that the IP is robust and already well tuned by the choices for r_s, R and v_0. The HOMO-LUMO gap is extremely sensitive to the softness parameter σ. The experimental data are also found in Table I for comparison. It indicates that $\sigma = 0.6\,a_0$ is the preferred choice concerning the HOMO-LUMO gap.

III. DIPOLE SPECTRA

As a first step, we will look at the optical absorption spectrum of C_{60} in terms of the dipole strength. To this end, we use TDDFT with the techniques of spectral analysis as outlined in [21]. We compare the results for the three values for σ under consideration.

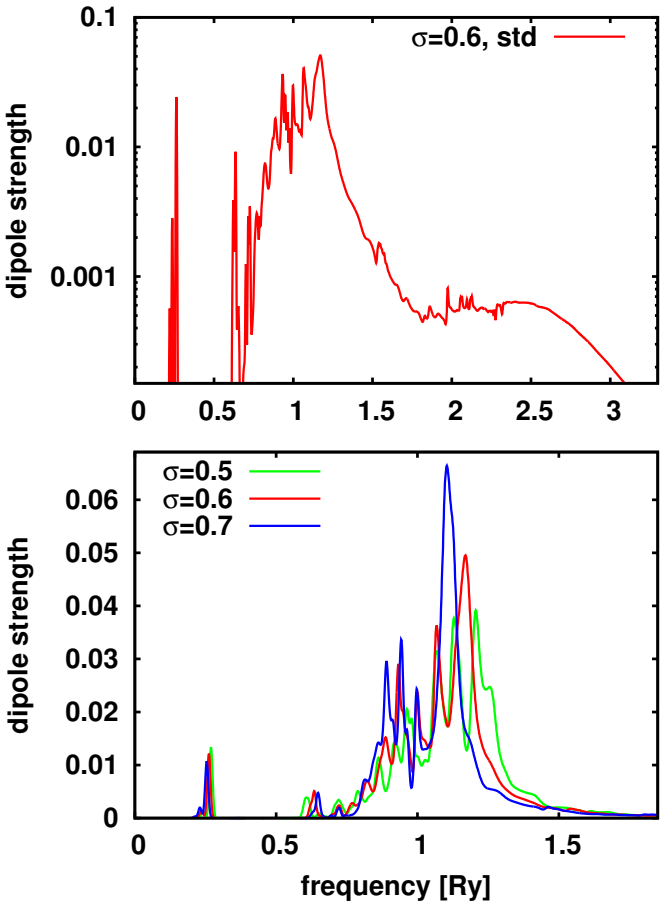

Fig. 1. Dipole strength for C_{60} in the soft jellium model under varying conditions. The lower panel shows the strength on a linear scale and compares the three cases with different surface width σ. The upper panel shows the spectrum for the standard case ($0.6\,a_0$) on logarithmic scale and for a broader frequency range.

Figure 1 shows the results. The low energy peak at about 0.3 Ry is surprisingly robust against variation of σ in spite of the fact that the HOMO-LUMO gap is strongly dependent on σ. This indicates that this low energy peak is of collective nature. The Mie surface plasmon peak resides around 1 Ry. It is strongly fragmented and broadened. The largest dependence on σ is seen in the upper branch of the surface plasmon peak. There is some down shift with increasing σ and a strong change of fragmentation. Only the case $\sigma = 0.7\,a_0$ displays one clean upper peak while the two other σ produce double and triple peaks. We have also checked the impact of box size and number of absorbing points. Comparing with results from a 50% larger box and another case with twice as much absorbing points (32 instead of 16 points). The spectral structures are practically independent of the box. Thus we have to conclude that they are a physical feature of the given jellium model. As these structures appear in the particle continuum, they correspond to scattering resonances. The upper panel shows the spectrum in logarithmic scale and over a larger frequency band. This points out even better the dominance of the Mie surface plasmon and it indicates furthermore a broad resonance

 ISBN: 978-1-61208-303-2

at about 2.5 Ry, probably a volume plasmon.

IV. Trend of anisotropy and emission time with laser frequency

The full angular distributions $d\sigma/d\Omega$ are functions of the angles θ and ϕ for each laser frequency $\omega_{\rm las}$. Spherical symmetry reduces this to a function of θ only. Even then, it is extremely hard to study systematic trends with such bulky observables. Fortunately, it turns out that the most characteristic pattern in the regime of weak laser excitations (one photon processes) is the anisotropy β_2. Indeed, the PAD cross section $d\sigma/d\Omega$ can be shown to be proportional to $1 + \beta_2 P_2(\theta)$, where P_2 is the second Legendre polynomial and θ the angle with respect to the laser polarization axis [12]. We will now investigate the anisotropy β_2 as function of laser frequency. For reasons of numerical convenience, we use here the softest model with $\sigma = 0.7\,{\rm a}_0$. The laser frequencies used here are all in a range above the IP of C_{60} and the intensities are moderate such that we deal with one-photon processes throughout. The PAD can thus be simply analyzed by means of the anisotropy parameter β_2.

Figure 2 shows observables from electron emission computed with the soft jellium model with surface width $\sigma = 0.7\,{\rm a}_0$. The intensity was kept constant throughout all frequencies. The upper panel repeats the dipole strength from TDLDA and compares it with the strength of the pure one-particle-one-hole ($1ph$) states as deduced from the static calculations. This shows that the Mie surface plasmon peak resides in a vacuum of $1ph$ states. A bunch of fragmented strength below the resonance is caused by the coupling to the many $1ph$ states there. The middle panel shows the total ionization $N_{\rm esc}(\omega_{\rm las})$. It follows nicely the trends of the dipole strength.

The lower panel finally shows the anisotropy $\beta_2(\omega_{\rm las})$. Large fluctuations are seen at the lower frequency side where we have the $1ph$ dominated states in the spectrum (see upper panel) and also the values are generally larger in this region. Above that $1ph$ region, the values drop to lower level and remain rather constant over a broad range of $\omega_{\rm las}$. The first three vertical dashed lines mark two minima and one maximum of β_2 while the fourth vertical line goes through the resonance peak. It is interesting to note that the minima of β_2 are related to the position of strongest slope upwards wings of the dipole strength before a peak. The maximum in β_2 seems to be related to a minimum in the dipole strength. Nothing special for β_2 can be spotted at the resonance frequency and along the right wing of the resonance.

It is known that the time profile of dipole oscillations and ionization depends on the laser frequency in relation to system resonances, see e.g. [22]. In order to allow tracking a frequency dependence, we reduce the time profile of ionization $N_{\rm esc}(t)$ to three key values: maximum slope $\partial_t N_{\rm esc}$, the time $t_{\rm max}$ at which maximum slope is reached, and the "final slope" $\partial_t N_{\rm esc}\big|_{t=t_{\rm fin}}$ at the end of the simulation time. The definition is illustrated in Figure 3. We see that the off-resonant case shows significant emission only during the laser pulse of 500/Ry while the resonant case is accompanied by long persisting dipole oscillations, which lead to emission after the pulse has died out. This feature is characterized by the final slope. Zero final slope indicates an off-resonant excitation. The figure also

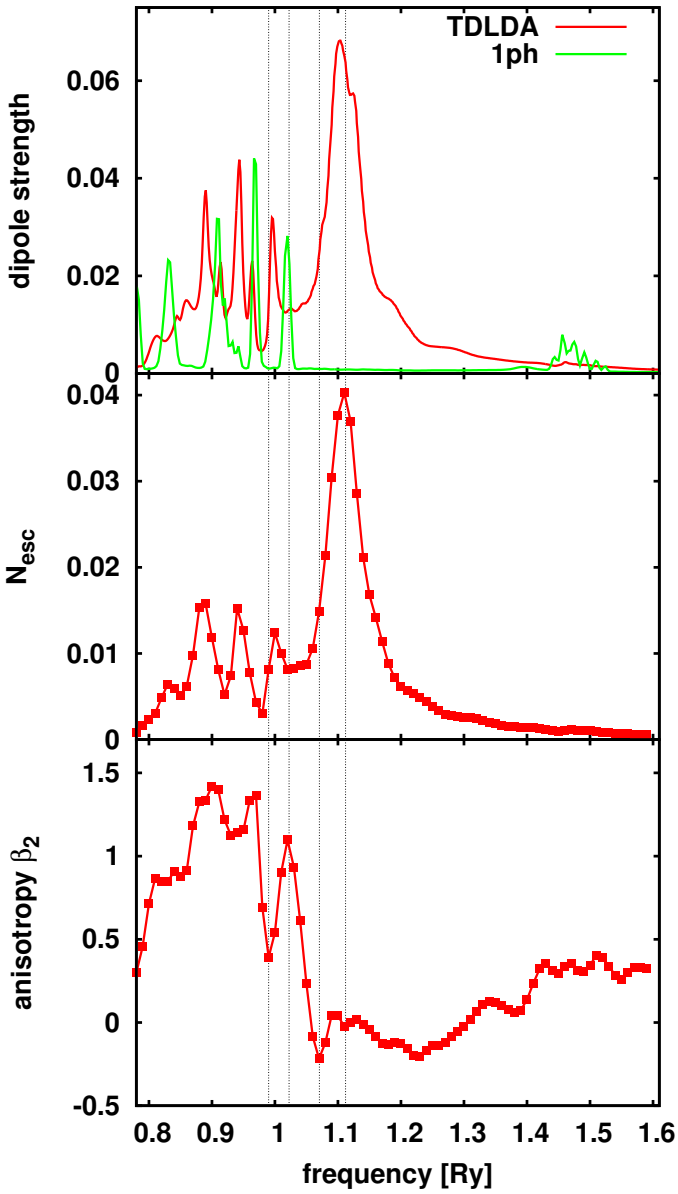

Fig. 2. Properties of electron emission after laser excitation as function of laser frequency $\omega_{\rm las}$. The soft jellium model with $\sigma = 0.7$ a_0 is used. The laser pulse had field strength $E_0 = 0.00034\,{\rm Ry/a_0}$ and pulse length $500/$ Ry. Lower: anisotropy β_2. Middle: ionization. Upper: dipole strength for full TDLDA and for pure $1ph$ excitations.

indicates that resonant emission is associated with some delay leading to later $t_{\rm max}$.

Figure 4 shows the three key values of ionization as function of laser frequency. The upper panel shows the time $t_{\rm max}$ where $N_{\rm esc}(t)$ has maximum slope. Peaks in dipole strength (resonances) are clearly related to delay in emission thus larger $t_{\rm max}$. However, the small peaks in the $1ph$ region make a much larger effect than the broad Mie surface plasmon peak. A similar behavior is seen in the maximum (relative) slopes as such, which are shown in the middle panel. It is plausible that large $t_{\rm max}$ correlate with low maximum slopes and vice versa. Large fluctuations reside in the region of $1ph$ strength. The lower panel shows the final slopes, evaluated at

 ISBN: 978-1-61208-303-2

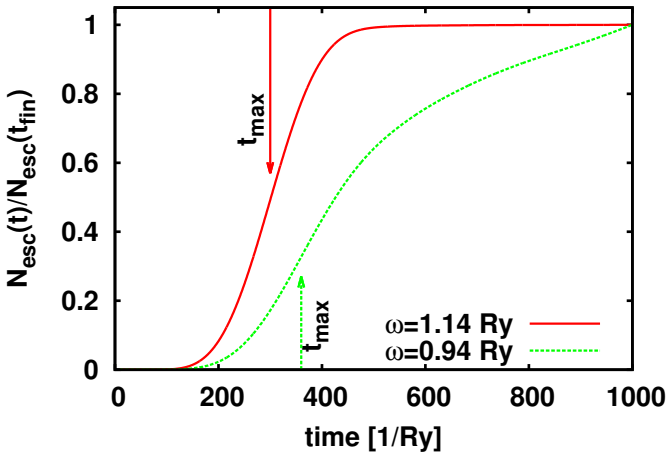

Fig. 3. Time evolution of ionization $N_{\rm esc}$ for one resonant ($\omega_{\rm las} = 0.94\,$Ry) and one off-resonant ($\omega_{\rm las} = 1.14\,$Ry) case. The time $t_{\rm max}$ at which maximum slope occurs is indicated for each case. The maximum and the final slope can be read off visually.

the end of the computation ($t_{\rm final} = 1000$/Ry). It indicates the amount of post-oscillations, which persist after the laser pulse is over. And again, we see large effects in the $1ph$ region, none at all at Mie plasmon resonance.

We have seen in the above discussion that the position of $1ph$ states relative to the resonance peak may have a decisive impact on the pattern of β_2 and slopes. We check this by comparing the soft jellium model used above ($\sigma = 0.7\,{\rm a}_0$) with the steep jellium model from Bauer et al [20]. The results are shown in Figure 5. The resonance position for the steep jellium is a bit higher. This is due to the fact that we use here 260 electrons, instead of 238 in the soft jellium. The important point is the relative position between $1ph$ strength and the resonance. And here it is clear that the steep jellium produces a much larger overlap between resonance and $1ph$ band. Moreover, the $1ph$ spectra of steep jellium are less bunched than those of soft jellium. (This may be a result from the coarse numerical reproduction of steep jellium on a finite grid.) The resonance is thus more strongly fragmented and more fuzzy for steep jellium. The anisotropy seems to yield at first glance different pattern. But the qualitative findings are the same: we see high β_2 with large fluctuations in the energy range of the $1ph$ bands but a smaller and more constant β_2 above the band. The final slope (right lower panel) confirms this sensitivity to the $1ph$ region. This also holds for the maximum slope and time thereof where fluctuations are correlated with the $1ph$ band and constant trends above. However, in these latter two observables we see much smaller fluctuations for the steep jellium. Altogether, this comparison shows the extreme sensitivity of the results to the detailed spectral fragmentation. The effects may be now understood qualitatively. But a quantitative prediction will require a very reliable model of C_{60}.

V. Conclusion

This first investigation, although preliminary, already provided several interesting conclusions. The soft jellium model delivers an acceptable description of C_{60} with $N_{\rm el} = 238$ electrons while allowing conveniently large grid spacings.

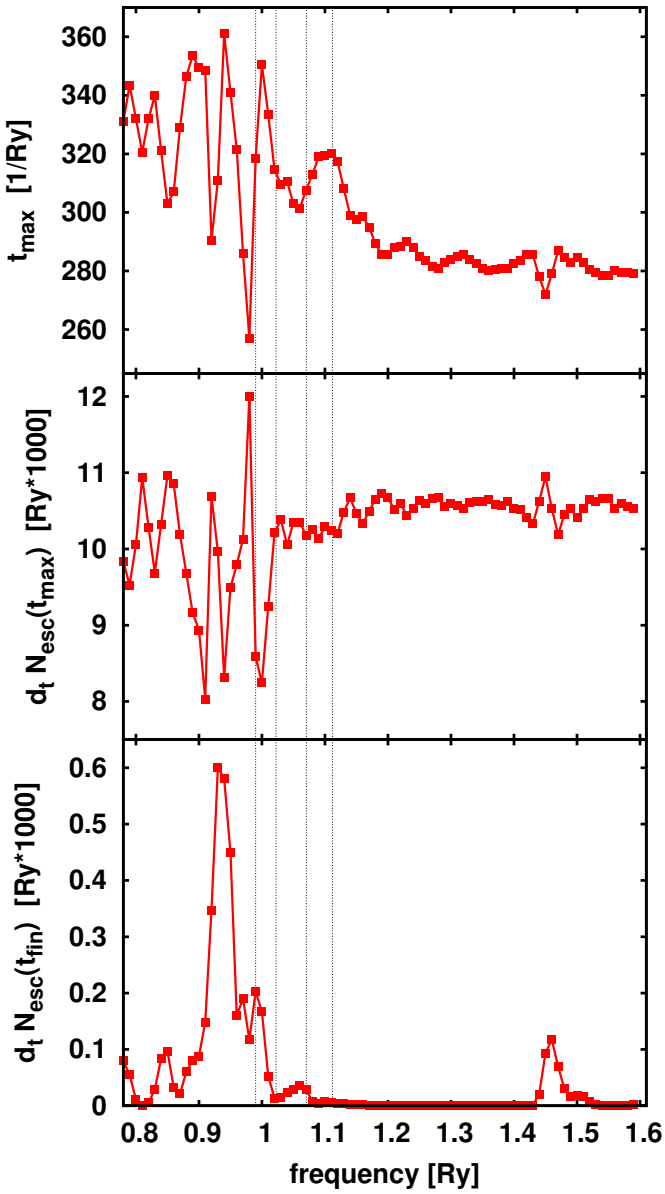

Fig. 4. Properties of the time profile of ionization as function of laser frequency $\omega_{\rm las}$. Jellium model and laser conditions were the same as in Figure 2. Lower: Final slope of $\partial_t N_{\rm esc}\big|_{t=t_{\rm fin}}$. Middle: maximum slope $\partial_t N_{\rm esc}$. Upper: time of maximum slope $t_{\rm max}$. The vertical lines are placed at the same frequencies as in Figure 2 to allow better comparison.

There is a significant fragmentation (depending on model parameters) of the surface plasmon resonance, which is caused by a high density of $1ph$ resonances in the continuum. A possible weakness is that the spherical model leads to a too pronounced structure due to the bunching of s.p. levels into degenerated angular momentum blocks. The lower symmetry of the actual fullerene structure may deliver a more diffuse sequence of resonances, which, in turn, could allow the surface plasmon to look more like one broad resonance peak. The question is what effect the bunching may have on the trends of the anisotropy parameter β_2. Comparison of results from steep with soft jellium indicates that more diffuse $1ph$ spectra reduce the amplitude of the fast fluctuations in anisotropy

 ISBN: 978-1-61208-303-2

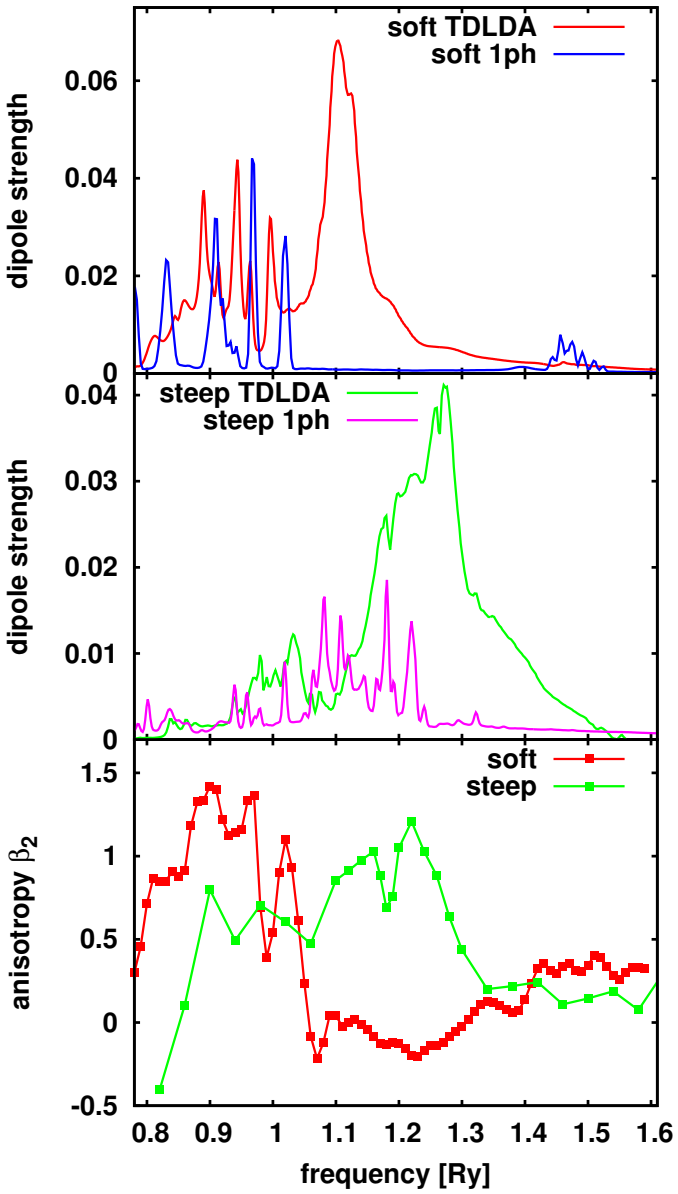

Fig. 5. Similar as Figure 2, but here comparing the soft jellium model $\sigma = 0.7a_0$ (red lines) with the steep jellium model of [20] (green lines). The dipole spectra for the two cases are shown in separate panels each one comparing full TDLDA with pure $1ph$ spectra. The lowest panel compares the anisotropies β_2 between steep and soft jellium.

and slopes. The soft jellium model allows robust and stable calculations of basic emission properties as anisotropy and emission time. The results confirm a relation between dipole strength and minima or maxima in the anisotropy as function of laser frequency. These effects are, however, much more pronounced in the regime of $1ph$ fragmentation than in the surface plasmon resonance. This qualitative result seems to be confirmed by calculations in the steep jellium model. The next step is certainly to explore these trends in a more detailed manner using a full ionic background and thus a full 3D description of the system. The first results of such more complete computations are presently being produced.

ACKNOWLEDGMENT

The authors thank Institut Universitaire de France and Humboldt foundation for support.

REFERENCES

[1] D. Turner, *Molecular Photoelectron Spectroscopy*. Wiley, New York, 1970.

[2] P. Ghosh, *Introduction to photoelectron spectroscopy*. John Wiley and Sons, New York, 1983.

[3] D. G. Leopold and W. C. Lineberger, "A study of the low-lying electronic states of Fe_2 and Co_2 by negative ion photoelectron spectroscopy," *J. Chem. Phys.*, vol. 85, pp. 51–55, 1986.

[4] D. G. Leopold, J. Ho, and W. C. Lineberger, "Photoelectron spectroscopy of mass-selected metal cluster anions. i. Cu_n^-, $n = 1 - 10$," *J. Chem. Phys.*, vol. 86, pp. 1715–1726, 1987.

[5] G. Ganteför, K. H. Meiwes-Broer, and H. O. Lutz, "Photodetachment spectroscopy of cold aluminum cluster anions," *Phys. Rev. A*, vol. 37, pp. 2716–2718, 1988.

[6] K. M. McHugh, J. G. Eaton, G. H. Lee, H. W. Sarkas, L. H. Kidder, J. T. Snodgrass, M. R. Manaa, and K. H. Bowen, "Photoelectron spectra of the alkali metal cluster anions: $Na_{n=2-5}^-$, $K_{n=2-7}^-$, $Rb_{n=2-3}^-$, and $Cs_{n=2-3}^-$," *J. Chem. Phys.*, vol. 91, pp. 3792–3793, 1989.

[7] J. C. Pinaré, B. Baguenard, C. Bordas, and M. Broyer, "Angular distributions in photoelectron spectroscopy of small tungsten clusters: competition between direct and thermionic emission," *Eur. Phys. J. D*, vol. 9, pp. 21–24, 1999.

[8] C. Bartels, C. Hock, J. Huwer, R. Kuhnen, J. Schwöbel, and B. v. Issendorff, "Probing the angular momentum character of the valence orbitals of free sodium nanoclusters," vol. 323, pp. 1323–1327, 2009.

[9] M. Kjellberg, O. Johansson, F. Jonsson, A. V. Bulgakov, C. Bordas, E. E. B. Campbell, and K. Hansen, "Momentum-map-imaging photoelectron spectroscopy of fullerenes with femtosecond laser pulses," vol. 81, p. 023202, 2010.

[10] H. Kroto, "Symmetry, space, stars and C_{60}," *Rev. Mod. Phys.*, vol. 69, pp. 703–722, 1997.

[11] P.-G. Reinhard and E. Suraud, *Introdcution to cluster dynamics*. Wiley-VCH, Berlin, 2003.

[12] P. Wopperer, B. Faber, P. M. Dinh, P.-G. Reinhard, and E. Suraud, "Orientation averaged angular distributions of photo-electrons from free na clusters," vol. 375, pp. 39–42, 2010.

[13] M. Marques, C. Ullrich, F. Nogueira, A. Rubio, K. Burke, and E. Gross, *Time Dependent Density Functional Theory*. Springer Berlin, 2006.

[14] J. P. Perdew and Y. Wang, "Accurate and simple analytic representation of the electron-gas correlation energy," *Phys. Rev. B*, vol. 45, pp. 13 244–13 249, 1992.

[15] C. Legrand, E. Suraud, and P.-G. Reinhard, "Comparison of self-interaction-corrections for metal clusters," *J. Phys. B: At. Mol. Opt. Phys.*, vol. 35, pp. 1115–1128, 2002.

[16] C. A. Ullrich, *J. Mol. Struct. (THEOCHEM)*, vol. 501-502, p. 315, 2000.

[17] P.-G. Reinhard, P. D. Stevenson, D. Almehed, J. A. Maruhn, and M. R. Strayer, "Role of boundary conditions in dynamic studies of nuclear giant resonances and collisions," vol. 73, p. 036709, 2006.

[18] A. Pohl, P.-G. Reinhard, and E. Suraud, "Angular distributions of electrons emitted from Na clusters," vol. 70, p. 023202, 2004.

[19] M. J. Puska and R. M. Nieminen, "Photoabsorption of atoms inside C_{60}," vol. 47, p. 1181, 1993.

[20] D. Bauer, F. Ceccherini, A. Macchi, and F. Cornolti, "C_{60} in intense femtosecond laser pulses: Nonlinear dipole response and ionization," vol. 64, p. 063203, 2001.

[21] F. Calvayrac, P.-G. Reinhard, and E. Suraud, "Spectral signals from electronic dynamics in sodium clusters," *Ann. Phys. (N.Y.)*, vol. 255, pp. 125–162, 1997.

[22] F. Calvayrac, P.-G. Reinhard, E. Suraud, and C. A. Ullrich, "Nonlinear electron dynamics in metal clusters," vol. 337, pp. 493–578, 2000.

 ISBN: 978-1-61208-303-2